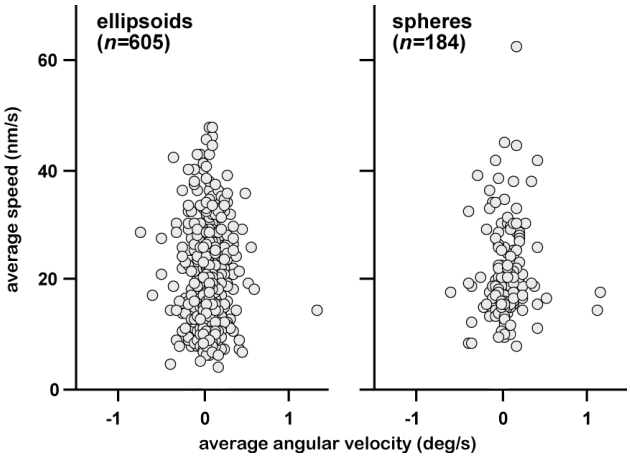

Supporting Figure S1. Spherical and ellipsoidal beads have similar motile behaviors. Spheres with an average diameter of 1 μm and ellipsoids with average dimensions of 1.8 x 0.8 μm have a similar speeds: mean of average speed = 19.9 nm/s, SD=8.7, n=605 for ellipsoids (left); 22.0 nm/s, SD=7.7, n=184 for spheres (right). In general, all of these uncoated beads tend to have relatively straight trajectories, as reflected by the mean of the magnitudes of average angular velocities: 0.10 deg/s, SD=0.11, for ellipsoids (left); 0.12 deg/s, SD=0.15 for spheres (right).

Supporting Text: Mathematical Model

We model ellipsoidal bead propulsion computationally in both 2D and 3D. In 2D, we simulate the combined viscoelastic-ratchet model. But in the more geometrically realistic 3D case, computer simulations of a deforming viscoelastic actin tail become forbiddingly long. Therefore, we treat the actin tail as rigid in 3D but with effective point-like elastic forces on the side to capture macroscopic elastic effects. Qualitative agreement of the results of these two models supports our conclusions.

I. 3D tethered ratchet model with elastic forces concentrated at the tail's edges

Model

A. Geometry

In 3D, the bead is represented as an ellipsoid with two identical short axes being 0.5 μm and a long axis being 1 μm. We define the bead's local coordinate system (*x, y, z*) so that the *x*- and *y*-axes pass through the bead's short axes and the *z*-axis passes through the bead's long axis. The geometry of the bead can be described as

$$\frac{x^2 + y^2}{0.5^2} + \frac{z^2}{1^2} = 1 . \qquad \text{[Eq.1]}$$

We assume that the ActA sites are randomly distributed on the surface of the bead without any spatial bias, and that the actin tail is formed only behind the rear-half of the bead surface that is opposite to the direction of bead movement, because small nascent filaments that are 'in the bead's way' are swept aside and not incorporated into the tail. We also define the tail's frame-of-reference (*X, Y, Z*) which is centered at the bead's centroid but with the *Z*-axis always being parallel to the bead's motion (**Fig. i**). In the tail's frame-of-reference, the immediate comet tail behind the bead is always along the *Z*-axis. We define the orientation of the bead in the tail frame as (θ, φ), where the yaw angle θ is the polar angle between the bead's long axis (*z*-axis) and the tail axis (*Z*-axis), and φ is the azimuthal angle of the bead's long axis about the *Z*-axis in the tail frame. We also define ψ as the rotation of the bead about its long axis. Then, the coordinates of the bead surface in the tail frame-of-reference, $\vec{r}$, can be obtained from the inverse of following Euler rotations:

$$\vec{r}_{loc} = R_z(\psi - \varphi) R_y(\theta) R_z(\varphi) \vec{r} , \qquad \text{[Eq.2]}$$

where $R_y(\theta) = \begin{pmatrix} \cos\theta & 0 & -\sin\theta \\ 0 & 1 & 0 \\ \sin\theta & 0 & \cos\theta \end{pmatrix}$ and $R_z(\varphi) = \begin{pmatrix} \cos\varphi & \sin\varphi & 0 \\ -\sin\varphi & \cos\varphi & 0 \\ 0 & 0 & 1 \end{pmatrix}$ are the rotation matrices about the *y*- and *z*-axes, respectively [1]; and $\vec{r}_{loc} = (x, y, z)^T$ is the coordinates of the point in bead's local frame.

For clarity, we illustrate the bead characterized by the yaw angle θ (positive in the clockwise direction) moving with speed V along an almost straight trajectory that curves with small angular velocity ω (positive in the counterclockwise direction) in **Fig. i.** Angles $\theta = 0$ and $\theta = \pi / 2$ correspond to propulsion in the *parallel* and *perpendicular* orientations, respectively. In other words, a bead's long axis is either perfectly *parallel* or *perpendicular* to the direction of motion.

B. Actin dynamics

The actin network in the comet tail consists of two dynamic actin arrays – transiently attached filaments resisting locomotion, and detached filaments that generate pushing forces. The processes of branching, capping, attachment, and detachment of actin filaments maintain the dynamic equilibrium between these arrays. We simulate a stochastic and spatially explicit version of the tethered ratchet model [2] describing these arrays: new filaments are first randomly created in the attached state at ActA sites that are scattered across the rear half of the bead surface (filaments that appear at the front half would not be incorporated into the tail, and thus, are irrelevant to force generation in the model). Attached filaments detach randomly and then remain detached until they are capped and disappear from the surface of the bead. The respective rates of all processes can be gleaned from the system of equations for the number of attached (n_a) and free (n_f) filaments in the nucleation model:

$$\begin{aligned} \frac{dn_a}{dt} &= k_{nuc}u + k_{att}n_f - k_{det}n_a, \\ \frac{dn_f}{dt} &= k_{det}n_a - (k_{att} + k_{cap})n_f. \end{aligned} \qquad \text{[Eq.3]}$$

Here k_{nuc} = 1000/s is the maximum filament nucleation rate over the bead surface, $u = 1 - (n_a + n_f) / N_{ActA}$ is the fraction of the ActA sites available for nucleating new filaments, N_{ActA}= 2000 is the total number of ActA sites on the bead [2], $k_{att} = 1$/s is the filament attachment rate, k_{det} is the detachment rate of the attached filaments, and k_{cap} = 0.1/s is the capping rate. Based on previous modeling [2], we use the following form for the velocity dependence of the detachment rate:

$$k_{det} = k_{det}^0 \left[1 + \left(V / V_0\right)^2\right] \Big/ \left[1 + \left(V / V_0\right)\ln\left(V / V_0\right)\right], \qquad \text{[Eq.4]}$$

where $k_{det}^0 = 5$ /s is the detachment rate at zero velocity, and $V_0 \approx 50$ nm/s is a characteristic velocity at which the detachment switches from the velocity-independent behavior at slow movement to velocity-dependent one when the bead moves faster.
In the simulations, 2000 ActA sites are evenly distributed on the bead surface with a spacing of approximately 50 nm. We assume a constant pushing filament density across the tail, rather than a constant density over the bead surface. Therefore, we add a projection factor, which is the dot product between the surface normal and the unit velocity vector $\left(-\vec{V} / V\right)$, to the generation rate of free filaments (we use notations $\vec{V}$ for velocity of the bead, and V for the respective speed). The result is that relatively more free filaments push at the rear of the bead, compared to the sides of the bead.

C. Balance of forces and torques

In the 3D model, each detached filament pushes with a force perpendicular to the surface of the bead (**Fig. i,** white solid arrows). These elongating filaments drum on the bead's surface as a result of Brownian motion and thus create a pressure normal to the local surface. Each attached filament pulls in the direction opposite to that of the bead's motion (**Fig. i**, white dashed arrows), which is parallel to the tail's axis. For the pushing filaments, we assume they are all pushing at the stall force

$$\vec{f}_{push}(\vec{r}) = -f_s \hat{n}(\vec{r}), \qquad \text{[Eq.5]}$$

where f_s = 3 pN is the stall force and $\hat{n}(\vec{r})$ is the outward normal unit vector of the ellipsoid's surface. The pulling force is assumed to be proportional to the local velocity of the bead's propulsion [2]:

$$\vec{f}_{pull}(\vec{r}, V, \vec{\omega}) = -k\left(\vec{V} + \vec{\omega} \times \vec{r}\right), \qquad \text{[Eq.6]}$$

where $\vec{\omega}$ is the bead's angular velocity and $k \approx 0.25\ \text{pN}\cdot\text{s/nm}$ is an effective drag coefficient depending on k_{det}^0 and the strength of attachment. Summing up all the pushing and pulling forces from all the attached and detached filaments gives the total force on the bead.

In order to balance the component of the total force that is perpendicular to the tail axis, we assume that a fraction of this sideways force is counteracted by the elastic bending of all attached filaments, while the rest of it is balanced by the local elastic reaction of the actin tail at the very side of the bead (at point A at the edge of the tail; see **Fig. i**). Mathematically, we add the force

$$\vec{F}_{elastic} = -\vec{F}_{\perp} = -\alpha \sum_{\substack{\text{attached} \\ \text{filaments}}} \vec{F}_{\perp} / n_a - (1-\alpha) \sum_{\substack{\text{local detached} \\ \text{filaments near A}}} \vec{F}_{\perp} / n_{local} \qquad \text{[Eq.7]}$$

to the sum of the filament forces in Eqs. 5 and 6. Here $\vec{F}_{\perp}$ is the unbalanced total sideways force, n_a is the total number of attached filaments (the balancing force is distributed equally among them), and n_{local} is the number of detached filaments in a small area at point A at the side of the bead. α is a weight factor which is adjusted to fit the data; good results are obtained for this factor being equal to 0.5.

The sub-piconewton viscous force on the bead ($F_{drag} \approx 6\pi\eta RV \approx 20\times0.01$ Pa·s×1 μm×0.02 μm/s =0.004 pN, where $\eta \approx 10\eta_{water}$=0.01 Pa·s) is negligible since it is much weaker than the filament forces. So, the mechanical condition for the bead's movement is that the total force equals zero:

$$\vec{F}(V, \vec{\omega}) = \vec{F}_{elastic} + \sum_{\substack{\text{attached} \\ \text{filaments}}} \vec{f}_{pull}(\vec{r}, V, \vec{\omega}) + \sum_{\substack{\text{detached} \\ \text{filaments}}} \vec{f}_{push}(\vec{r}, V) = 0. \qquad \text{[Eq.8]}$$

The total torque can be computed by summing up all the cross-products between individual force vectors and the corresponding position vectors in the lab coordinates. The total torque has to be equal to zero:

$$\vec{T}(V,\vec{\omega}) = \vec{r}_A \times \vec{F}_{elastic} + \sum_{\substack{\text{attached} \\ \text{filaments}}} \vec{r} \times \vec{f}_{pull}(\vec{r}, V, \vec{\omega}) + \sum_{\substack{\text{detached} \\ \text{filaments}}} \vec{r} \times \vec{f}_{push}(\vec{r}, V) = 0 . \qquad \text{[Eq.9]}$$

Together, Eqs. 8 and 9 allow finding the speed and angular velocity for the bead in the framework of the lab/actin tail. Because the beads in our experiment are confined in a flat chamber, in our model we further restrict the motion of the bead's centroid in a 2D plane in the lab frame while the bead's rotation is still in a 3D space.

D. Lipid-coated beads

As a lipid-coated bead is propelled forward, molecular complexes that attach to filaments are likely to be 'swept' backward. The distribution of attached filaments therefore becomes significantly biased rearward relative to the distribution of pushing filaments. To simulate this effect, we allow the ActA sites to diffuse on the bead surface, and to be pulled backward by attached filaments. Specifically, the displacement of an ActA site at $\vec{r}$ within a time interval Δt is postulated to be:

$$\Delta\vec{r}_{ActA}(\vec{r}) = \begin{cases} \left[\vec{V} \times \hat{n}(\vec{r})\right] \times n(\vec{r})\Delta t + \Delta\vec{r}_{rand} & \text{if the site is attached,} \\ \Delta\vec{r}_{rand} & \text{if the site is detached,} \end{cases} \qquad \text{[Eq.10]}$$

where $\Delta\vec{r}_{rand} = \sqrt{4 D_{ActA}\Delta t}\cdot\hat{e}$ is the random displacement of the ActA site due to the effective diffusion with the diffusion constant D_{ActA}; $\hat{e}$ is a random unit vector in the plane of the bead surface at position $\vec{r}$. We estimate the value of D_{ActA} from our observation that about 10 % enrichment of ActA is at the rear of the moving lipid-coated bead. By solving the simplified 1D drift-diffusion equation for the ActA density $D_{ActA}[\text{ActA}]'' - v[\text{ActA}]' = 0$ with the approximate values of the velocity and rear/front ratio of the ActA density, we estimate $D_{ActA} \approx 0.01\,\mu\text{m}^2/\text{s}$.

E. Curvature of the bead's trajectory and angular velocity

Fig. ii shows our approach to determining the tail curvature and the resulting angular velocity of the bead's centroid in the lab frame-of-reference. Let us start with points A and B (**Fig. ii, panel A**), which are the left and right boundaries of the tail on the bead surface, respectively. Within the time interval Δt, if the bead rotates with rate ω, then the bead will rotate by an angle $\Delta\theta = \omega\Delta t$ in the counterclockwise direction. As a result, point A will move 'into the tail', while the point B will move 'away from the tail'. We assume that existing filaments at the left edge of the tail can reach and establish contact with some area of the bead that is not previously covered by actin, so that the new tail edge on the left of the bead (A'') is located between the former edge (point A) and the farthermost possible point of contact (point A') of the 'old' existing tail (**Fig. ii, panel B**). Similarly, existing filaments at the right edge of the tail (point B) will have to recede to point B'' if they lose contact with the turned bead in the absence of any actin tail dynamics. Otherwise, the bead's turning could lead to the tail's localization towards the front of the moving bead, in which case the elastic forces in the tail will cause local brakeage and realignment of the tail's boundaries.

We make the assumption that the new boundaries of the tail, A'' and B'', are located in the middle of points A and A' and B and B', respectively, so that the increase of the tail-contacting area on the left equals the decrease of that area on the right (**Fig. ii, panels B, C**). There is no guarantee that the left and right sides of the bead always have the same amount of changes in the areas. More likely, certain force and kinetic balances will predict a numerical ratio between these incremental areas. However, in the absence of an explicit model for these balances, we decide to go with the simplest possibility. Other ratios still give the same sign of the angular velocity.

The locations of A'' and B'' can be obtained from the following two conditions: equal changes in the tail-contacting surface on the left and right of the bead, and tangents to the bead surface at A'' and B'' being parallel to each other (**Fig. ii, panel C**). Then, the change in the direction of tail growth is $\Delta\theta' = \Delta\theta / 2$, which determines the angular velocity of the tail's turning in the lab frame-of-reference to be $\omega / 2$. In the tail frame-of-reference, the angular velocity of the bead, or equivalently, the angular rate of turning of the yaw angle, is also $\omega / 2$. Thus, this model predicts that the angular velocity of the bead's centroid in the lab frame-of-reference and the changing rate of the yaw angle are comparable in magnitude and have the same sign.

In the simulations, the turning of the bead's trajectory is determined by the turning of the tail in the lab frame-of-reference. Since the latter is coupled to the change in the yaw angle, the resulting time-series of these angles give us the relation between the bead's angular velocity and yaw angle.

Results

Linear velocity as a function of yaw angle: Numerical simulations of Eqs. 3-9 predict that the Z-component of pushing force for beads with perpendicular orientations is, on average, 1.2 times of that for beads with parallel orientations. Since a bead's speed, V, is proportional to the pushing force, the ratio of bead's velocity between the two orientations is also about 1.2. This is in semi-quantitative agreement with our observations, according to which the respective speed ratio is close to 1.2.

Lipid-coated beads: We use the 3D model to simulate the *in silico* lipid-coated beads. The results for the yaw angle distribution are in good agreement with the observation data (see **Fig. iii**): the increased motility of ActA on the surface of lipid-coated beads leads to a bias of beads' rotation toward the parallel orientation. This occurs because the points of attachment between filaments and ActA are shifted to the rear, and the rearward force is mostly applied at the rearmost part of the bead. Therefore, a torque is generated to align the bead into its parallel orientation. The resulting angular velocity of beads has greater overall magnitude comparing to that of uncoated beads. The fraction of the yaw angle that is associated with a positive angular velocity, which turns the bead into its parallel orientation, is also higher for lipid-coated beads. Effectively, randomly oriented beads have greater chances to turn into the parallel orientation with greater angular velocities. As a result, more lipid-coated beads move in the parallel orientation, and fewer in the perpendicular orientation compared to uncoated beads.

Frequency of spontaneous yaw angle switching: We observed experimentally that about 89% of beads did not spontaneously switch orientations during the 17 min period of each time-lapse sequence; 9% switched once; and 1.5% switched twice (see **Table 1**, main text). This data fits very well the Poisson distribution for the random, memory-less switching [3] with frequency of about 1/170 min. In the 3D simulations, we find that the frequency of spontaneous switching between parallel and perpendicular orientations is very low (in the range of one per tens of minutes), which is in semi-quantitative agreement with the data (computer-time-consuming nature of the simulations did not allow gathering accurate statistics). Below, we present analytical estimates providing insight into the switching mechanism (Section VII).

II. 2D model of the viscoelastic actin tail with individual filaments at the bead-tail interface

A. Actin dynamics and forces

We model the autocatalytic branching of filaments according to the model previously described in [4]: the total branching rate (1/s/μm×(bead circumference)) is constant, while local filament creation rate is proportional to the local density of existing actin network nodes that are within 200 nm from the bead surface. We also include a spontaneous filament nucleation process with a similar total rate (1/s/μm×(bead circumference)). In the model, filaments are treated in a coarse-grained fashion such that each filament represents an actin array consisting of many individual filaments. We do not track the orientation of each individual filament, because the computer simulation will be highly time-consuming. Instead, we assume that the effective filament arrays are always normal to the local bead surface. We also do not explicitly include the 70 degrees between mother and daughter filaments. When a daughter filament array branches off a mother filament array, we slightly shift its location from the mother array to represent the effective lateral propagation of the branched actin networks [4]. The speed of this shift is chosen to be a random fraction of the free-filament polymerization speed, because the speed of the network propagation should not exceed the polymerization speed of free filaments. The daughter array shifts in a random direction from the mother array along the bead surface, as the direction of the actin propagation is unbiased.

To maintain a persistent bead's motion, we assume that the filament nucleation rate is higher at the rear of the bead compared to that at the front. This effect could result from actin arrays at the front of the bead being swept away by the flow around the bead before the network at the front could mature. We choose the front-to-back ratio of the nucleation rate to be 1:2. Nascent filaments can be in either attached or detached state, with dynamic equilibrium between them; the rates of transition from one state to the other are $k_{att} = 1/\text{s}$ and $k_{det}^0 = 5/\text{s}$. Each newly created filament immediately becomes a part of the existing node-spring network by treating the pointed end of the filament as a new node in the network. Each new node connects to 3 to 4 neighboring nodes within 100-500 nm (respective selection of the nodes is random, but such as not to choose neighbors that are

too close to each other or are in the same direction from the nascent node). Each free filament attaches to the bead surface with a rate $k_{att} = 1/\text{s}$ if its barbed ends is in contact with the bead surface. Each attached filaments can detach from the bead surface and become free with a rate that increases exponentially with the stretching force: $k_{det} = k_{det}^0 \exp(-f / f_0)$ where $f < 0$ is the stretching force on the filament and $f_0 = 1.5\,\text{pN}$ is a force scale. Each free filament gets capped with a constant rate $k_{cap} = 0.1/\text{s}$. When the filament array is capped, the actin network node associated with it is kept until that part of the network disassembles (we choose the disassembly rate to be 0.008 s^{-1}, which corresponds to an average filament lifetime of about 120 s, long enough not to affect the network around the bead). The growth of free filaments follows the Brownian ratchet theory: filament arrays elongate with the rate $v = v_m \exp(-f / f_0)$ where $f > 0$ is the pushing force and $v_m = 50\,\text{nm/s}$ is the free polymerization rate.

Filament arrays are treated as linear elastic springs so that they can exert forces on the bead depending on their deformations. The spring constant for all filaments is assumed to be the same, $k_s = 300$ pN/μm. If a filament array is attached and stretched, it exerts respective pulling force. If the growing end of an array penetrates the bead's surface, the array is considered to be deformed by the penetration length, and so exerting respective pushing force. Forces that exert on the filament arrays automatically apply to the connected node-spring network and cause stress in the network. The deformation of the network, in turn, influences the interactions between the filaments and the bead. In order to model lipid-coated beads, the tangential components of the forces acting on the attached filaments are nullified, while the normal force components are kept. Indeed, the tangential forces simply move ActA attachment points until the forces are relieved.

B. Network dynamics and forces

The actin network of the tail is treated as a node-spring meshwork. Nodes represent the effective network cross-links, while springs represent the deformable actin gel. All springs have the same spring constant, $k_s = 300$ pN/μm, which, considering effective hundreds of nanometers distance between the nodes, corresponds to the effective Young's modulus of the network of the order of 10^3 Pa [5]. When a new node (filament array) is created, all the links that connect it to neighboring nodes are assumed to be un-deformed, with rest lengths being the distances from the node to its respective neighbors. Springs can snap if the stretching force is beyond the threshold value, $f_{br} = 15\,\text{pN}$, representing either actual filament breaking or rupture of cross-links between the filaments. The nodes disappear at a constant rate, $k_{dis} = 0.008\,\text{s}^{-1}$, representing the disassembly of the actin network. The characteristic lifetime of the actin network is therefore $1/k_{dis} \approx 120\,\text{s} = 2\,\text{min}$.

The nodes are moved as follows. The net force that springs applied to the *i*-th node, $\vec{F}_i$, leads to the node's shift by $\Delta\vec{r} = \vec{F}_i / (k_s n_i)$, where n_i is the number of springs connected

to this node. Such shifts are repeated until the all nodes' positions converge to mechanical equilibrium. Furthermore, nodes with a distance to the bead surface greater than a threshold of 1 μm are immobilized. This represents attachment of the older part of the tail to the coverslip. This attachment simplifies calculations considerably, while not affecting the results in a qualitative way because the actin network deformations are important only within the part of the tail closer to the bead's surface than characteristic bead's size.

C. Bead movement

We approximate bead shape with an ellipse of aspect ratio 2. The translational and rotational movements of the bead are determined by the force and torque balances, respectively. During each time step, the displacement and rotation of the bead satisfy the condition that both total force and total torque from all the interacting filaments are zero, exactly as in the 3D model.

Results

Supporting Videos 8 and 9 illustrate that in our simulations the bead is bi-stable, moving either in the parallel or perpendicular orientation, with infrequent switches between the orientations, in agreement with our observations. Simulations of lipid-coated beads show that they are also more likely to move in the parallel orientation. The resulting distributions of yaw angles are reported in the main text (see **Fig. 4B, main text**). Also, the simulations further illustrate that the beads initiate the motility and break through the 'actin cloud', in the parallel orientation, agreeing with our observations.

This result also agrees with theories in [5-7], where respective symmetry breaking is studied for spherical beads and the 'rubber stack' model of symmetry breaking is suggested. According to this model, the first layer of the actin gel grows around the bead in a stress-free manner and forms a thin spherical shell at the bead's surface. Then, a nascent layer of the gel grows at the surface pushing the older actin shell outward. This deforms the outer actin layer so that a tangential stress stretching this outer layer is generated, while the inner layer is compressed radially.

For a fixed gel thickness, the tangential stress at the outer layer is estimated to be proportional to the local curvature of the bead surface [7]. For an ellipsoidal bead, the maximum surface curvature is at the two poles. Therefore, as new actin gel grows from the bead surface, the outer layer near the two poles experiences maximum tangential stress and is most likely to rupture. This local perturbation is unstable: as the actin shell thins out near the poles, the tangential stress of the gel increases at the same location, leading to an exponentially amplified rupture [7] of the actin gel near the two poles. As a result, the actin layer at the poles is thinnest and most vulnerable to fluctuations. When the actin gel ruptures near one pole, the rest of the gel relaxes which greatly reduces the chance of rupture at the opposite pole. The bead will then be pushed out the actin cloud in the parallel orientation through the 'hole' in the gel. Our qualitative observations are consistent with this scenario: before a bead breaks symmetry, the actin fluorescence

around that bead seems to fluctuate for minutes to tens of minutes. When actin starts to thin out and break at one pole, bead's motility starts.

III. Predictions of alternative force-generation models

As a comparison to the 2D viscoelastic model, we simulate separately two 2D models: the simplest variant of the elastic propulsion theory and the tethered ratchet model with a rigid tail that lacks the effect of the elastic forces. The models are built as follows. For the elastic model, we consider, instead of the autocatalytic actin nucleation, a constant nucleation rate (1/s/μm×(bead circumference)) along the bead surface. Because of this condition, effectively constant pushing forces locally normal to the bead's surface are applied at the actin-bead interface, which is similar to the assumption in the elastic propulsion theory. In the tethered ratchet model, we simulate autocatalytic branching, growth, capping, attachment and detachment of hundreds of actin filaments (individual filaments, not effective arrays). The filaments are branched at the proper 70 degrees angle between mother and daughter filaments. The capped filaments are considered rigid and immobile in the lab coordinate system. The uncapped filaments that are in contact with the beads surface are considered to be the elastic rods. We consider actual elastic deformations of such individual filaments. For the free filaments, the boundary condition for the barbed ends is zero tangential forces, and for the attached filaments – fixed coordinates of the barbed ends. Solution of the elasticity theory equations give the elastic forces exerted by each such filament on the bead. To compute the bead's movement, we compute at each step the total force and torque and displace and rotate the bead iteratively until the total force and torque are equal to zero.

The elastic propulsion theory suggests that actin growth generates a radially stretched layer of gel around the bead, and that the bead is squeezed forward by this layer, propped up by more relaxed actin at the rear. This theory implies that the pushing forces are mostly concentrated at the bead poles *A* and *B* (**Fig. i**). With this geometry, such forces exert a torque that will always turn the bead into the parallel orientation. Numerical simulations of this model confirm this intuition: the beads break the stability in the parallel orientation and continue to move in the parallel orientation, as is evident from the **Supporting Video 6**.

Numerical simulations of the tethered ratchet model for the rigid tail, without the effect of elastic forces, show that the bead moves in the perpendicular orientation and never turns into the parallel one, regardless whether new filaments are branched from existing filaments (**Supporting Video 4**) or spontaneously nucleated at the back of the bead (**Supporting Video 5**). The qualitative explanation for this effect is that the bead in a skewed orientation experiences a net force pushing it off the center of the tail, so that at the edge of the bead-tail interface, nascent actin filaments propagate faster along the flatter side of the bead and slower along the curvier side. As a result, the actin network spreads along the more flat half of the bead surface keeping the bead in the perpendicular orientation.

For the lipid-coated beads, both models give the same predictions: as the pulling forces are swept to the rear creating the torque that tends to turn the bead into the parallel configuration, this increases the stability of the parallel orientation in the elastic model, and decreases the stability of the perpendicular orientation in the ratchet model. Obviously, as these two models separately do not predict the bimodal yaw angle distribution, the question about the orientation switching frequency is irrelevant in their frameworks. Finally, the elastic model gives the same prediction about symmetry breaking as the combined model. The ratchet model cannot address this question because of the rigid nature of actin tail in this model.

We consider qualitatively a number of other possibilities as follows. The actin end-tracking model [8] implying yet-to-be-discovered molecular motors at the tips of the filaments leads to the co-localization and, probably, co-alignment of the pulling and pushing forces. It is not clear how to explain any torque under such assumptions. Besides, the greater linear speed of the lipid-coated beads and bias of ActA to the rear of such beads is hard to explain in the framework of this theory, without any spatial separation of pulling and pushing filaments.

Since we observed that there is a faint actin ‘cocoon’ all around the motile beads, we consider the possibility that a strong resistive force originates from continuous ‘breaking’ of the beads through this actin layer. However, semi-quantitative examination of the respective forces failed to explain the bi-stable angular equilibrium of the bead orientation. Besides, beads with both thick and thin actin ‘cocoon’ around them behaved the same.

We also consider the possibility that most of the pushing forces are concentrated at the rearmost point of the bead’s surface and that filaments at the sides are ineffective. However, this scenario leads to the pushing torque invariably turning the bead into the perpendicular orientation, and no assumptions about pulling force distribution are able to restore the bi-stable angular equilibrium of bead orientation.

Finally, one could imagine a peculiar spatial, or even more complex spatiotemporal separation of pushing and pulling forces that would lead to the bi-stable equilibrium in orientation of the motile ellipsoidal beads. For example, if there are more attached filaments at the ‘poles’ and ‘equator’ of the beads, and more pushing filaments at the circular bands between the poles and equator, simulations indicate that the bi-stability is possible. Another possibility is a peculiar dependence of the attachment-detachment dynamics of filament tips on not just the local curvature of the beads surface, but on the derivative of this curvature. However, it is very hard to imagine the biophysical mechanisms that would enable such contrived effects. Similarly, we examine a remote possibility that the pushing forces are aligned with the tail’s axis, or that the pulling forces are not aligned with the tail’s axis, and found that these assumptions do not explain the data either.

IV. Future applications of the hybrid mesoscopic model

The hybrid mesoscopic model is applicable to the force-velocity relation for actin networks growing against rigid surfaces in *in vitro* experiments. It is possible that viscoelastic recoil of the network combines with ratchet forces at the actin-surface interface to produce observed nonlinear and hysteresis-like force-velocity relations. Also, it would be useful to apply the model to the actin network adhering to the compliant substrate and growing against flexible plasma membrane under tension. A number of studies established that retrograde flow of the actin network contributes to the rate of cell protrusion, but the respective viscoelastic effects coupled to individual pushing filaments were never consistently considered.

V. Effect of an actin gel layer around the bead

If the actin gel at front is thin and uniform and the lateral elastic stress is constant in the front gel (**Fig. iv, panel A**), the normal stress will be proportional to the local curvature of the bead (Laplace's law): $f_{\text{res}}=\alpha\kappa$, where α is a constant being proportional to the lateral stress and κ is the local curvature of the bead surface. To calculate the total force F, we define coordinates x'-y' such that the x'-axis is parallel to the front-back boundary AB and the y'-axis is pointing towards the front side of the bead (**Fig. iv, panel B**). We also define ψ to be the angle between the tangent of the bead surface at P and the positive y'-direction. Let ψ_{A} and ψ_{B} be the values of ψ at points A and B, respectively, we have $\psi_{\text{B}} = \pi - \psi_{\text{A}}$. Since $\kappa = \mathrm{d}\psi/\mathrm{d}s$, where s is the arc length along the surface, the x'- and y'-components of total force are

$$F_{\text{res},x} = \int_A^B f_{\text{res}} \cos\psi \, ds = \alpha \int_{\psi_{\text{A}}}^{\psi_{\text{B}}} \cos\psi \, d\psi = 0,$$

$$F_{\text{res},y} = -\int_A^B f_{\text{res}} \sin\psi \, ds = -\alpha \int_{\psi_{\text{A}}}^{\psi_{\text{B}}} \sin\psi \, d\psi = -2\alpha \cos\psi_{\text{A}} < 0.$$

The total resisting force F_{res} is always along the negative y' direction, which is always perpendicular to line AB and points towards the back of the bead.

The total torque produced by the compression forces about the bead's center is zero. This can be seen in **Fig. iv, panel A**. Let point C be the symmetric point of A about the bead's long-axis. Because of the symmetry, the torque from compression forces between A and C is zero, and the torque from compression forces between B and C is also zero. Thus, the total torque from the compression forces at the front is zero. Similar argument shows that if the origin of the force is not elastic but pushing from ratchet mechanism, the total torque would be zero.

The resisting force, however, will affect the bead's torque balance indirectly. That is because F_{res} typically has a component along the short-axis of the bead, which is against the sideways pushing force from the tail and helps relieve the local elastic force. As a result, the torque from F_{elastic} is smaller, which reduces the tendency of bead's moving along its long-axis. Therefore, the existence of a thin gel at the front of the bead tends to align the bead to move along its short-axis. If the origin of the force is from the ratchet

mechanism, then the effect discussed in this paragraph slightly reduces the bias toward the orientation along the bead's short axis.

If the actin gel covering the front of the bead is non-uniform, it is likely to generate a torque on the bead. One possibility is that gel exists when the angle between the surface normal and v is greater than a certain critical angle ϕ_c (points C and D in **Fig. iv, panel C**). This could result from the "brushing" of the surrounding fluid on the gel. If the gel between points C and D exists, the total torque from the front gel is zero. Since the gel between C and D produce a torque that turns the bead to the perpendicular direction (τ^* in **Fig. iv, panel C**), the torque from the rest of the front gel should align the bead to move along its long-axis. This conclusion remains the same whether the force is produced by elastic or ratchet mechanism.

The other possibility is that gel at front tends to rupture near highly-curved surface due to high lateral stress. Then, the thinning of gel is symmetric about the long-axis of the bead. The resulting force and torque are zero, having no impact on the orientation of the bead. From this analysis, we conclude that gel at front of the bead may have different impact on the orientation of the bead, depending on the property and configuration of the gel, but as long as the gel is thin, the influence is likely to be small.

VI. Temporal sequence of changes in motion, orientation, and actin density

In the following text we qualitatively explain the observed sequence of events: turning or change in direction in the bead's trajectory (angular velocity) → actin accumulation on the inner side → change in bead orientation with respect to the comet tail (yaw angle).

The number of attached filaments is significantly smaller than that of free filaments, and so the relative fluctuations of number of the attached filaments are expected to be significant. This leads to fluctuations in the attached/free filament ratio that causes unbalanced forces and growth speeds at the two sides of the bead. Specifically, the side with a higher fraction of attached filaments will move slower than the other side, causing the trajectory turning. We suggest that this consequence of the fluctuation of the attached filament number is the beginning of the sequence of the observed changes.

As the bead changes direction and curves in its trajectory, the inner side of the bead moves more slowly than the outer side, resulting, according to the model, in a lower filament detachment rate and thus in a higher density of attached filaments on the inner side of the bead. In addition, the slower relative motion between the inner bead surface and the tail reduces the effect of the free filaments growing past the surface and 'leaving' it, further increasing the filament density at the inner side. The time lag between the trajectory turning and the accumulation of actin at the inner side of the bead is roughly the actin network turnover time, which is estimated to be about 20 s, consistent with the experimental observation.

Next, the redistribution of the actin density around the bead will lead to the bead's reorientation relative to the tail, after the oscillation of the attached/free filament ratio is reduced. The reorientation of the bead with respect to its tail is driven by both the torque and the reorientation of actin tail along the bead surface. The speed of turning is also affected by the resistance from the actin gel around the bead: the bead needs to move through the cocoon of existing gel before it can turn. Thus, changes in yaw angle happen after changes in the direction of a bead in a trajectory and actin redistribution. For a bead moving at a speed of 30 nm/s, the time required to advance a sub-micron distance (a fraction of the bead's size) is on the order of 10 s. We estimate that the time lag for the change of yaw angle is comparable to this time interval, which is consistent with the observed 10 s delay.

VII. Frequency of bead orientation switching

Bead orientation switching between the parallel and perpendicular orientation can be explained as follows. In addition to the turning from torque and geometric effect, there is turning caused by fluctuation in the actin networks. Considering N filaments pushing against the bead rear surface, the fluctuation in filament numbers from the left to the right sides of the bead is about $\sqrt{N}$. On average, these fluctuating filaments tend to push the bead at an angle of $\pi/4$ away from the current direction of motion, causing random turnings of the bead, while the rest filaments push the bead along its previous direction. The net angular change in the direction of motion is $\Delta\theta \sim (\pi/4)(\sqrt{N}/N) = \pi/4\sqrt{N}$. The duration of this bias is related to the actin turnover time τ_0, which is obtained from stability analysis of Eq. 3. The rotational diffusion constant for this turning can be estimated as $D = \Delta\theta^2/2\tau_0 \sim \pi^2/32N\tau_0$. With actin fluctuation alone, the average time for a bead to reach halfway of the orientation-switching is $t_0 = (\pi/4)^2/2D \sim N\tau_0$. The relative rotation between the bead and its tail is also affected by both the torque from the tail and the reorientation of the actin tail along the bead surface. Since the orientation of beads have bi-stability, the angular velocity of the bead with respect to its tail can be approximated as $\omega \approx \omega_0 \sin(4\theta)$, meaning that beads with $0 < \theta < \pi/4$ tend to rotate towards its long-axis while beads with $\pi/4 < \theta < \pi/2$ tend to rotate towards its short-axis. Therefore, the total time for a bead to achieve half of the orientation switching can be estimated from the Arrhenius equation (assuming effective diffusion-drift process in the angular space): $t = t_0 \exp\left(\frac{1}{D}\int_0^{\pi/4} \omega\, d\theta\right) \approx N\tau_0 \exp(16N\omega_0\tau_0/\pi^2)$, where the exponent in the second term represents the maximum "barrier height" for the rotation. For the beads with $N \approx 900$, $\omega_0 \approx 0.1$ deg/s and $\tau_0 \approx 1\,\text{s}^{-1}$, we get $t \sim 100 - 200$ min, which agrees well with the observed time interval for switching t ~ 170 min.

VIII. Bead orientation during symmetry breaking

The differences between our finding that the bead starts moving and breaks through the symmetric layer of actin gel in the parallel orientation and a previous published observation [9] can be due to experimental differences. First, this previous study [9] involved a reconstituted system consisting of purified proteins, which probably had slower actin depolymerization dynamics than the cytoplasmic extracts used in our study. Because of the faster actin depolymerization rate in our case, the elastic stress in the network decreases faster and the stress can be more local, not spreading across the whole bead-actin interface. If this is the case, the local elastic stresses correlate with local interface curvature, which is highest near the bead's poles, where we observe the symmetry breaking. If the stress spreads more globally in the case reported in [9], then the local curvature variations matter less than the hoop stress that develops around the bead's 'equator' and dominates stresses in all other directions. Such hoop stress, as was shown in [9], leads to the linear break along the long axis of the bead at its more flat side and emergence of the bead from the actin cloud in the perpendicular orientation.

The second reason could be differences in geometry. In our study, ~1 μm beads are confined in a slide-chamber only ~2 μm deep. But in [9], ~5 μm beads are placed in a 15.5 μm deep chamber. The ratio of the chamber depth to the bead size is 2 in our case and 3 in [9]. Therefore, we argue that beads in our study are confined in a quasi-2D environment, while those in [9] are in a more 3D environment. Our 2D simulations predict the symmetry break in the parallel configuration, and this geometry resembles the experimental configuration of the current study more closely. The symmetry breaking process is more 3D in [9], and the 3D model used in [9] indeed predicts symmetry breaking through the actin cloud in the perpendicular orientation, because the dominant hoop stress in the actin gel is essentially a 3D phenomenon.

IX. Rapid trajectory turning behavior of lipid-coated beads

In the text, we have a qualitative explanation for the observed faster angular speed of lipid-coated beads. This explanation is based on the spatial separation between the maxima of the ActA distribution (which is at the rear pole of the bead) and of the actin distribution (which is skewed to the inner side of the bead relative to the trajectory). Our model can produce such separation only transiently and briefly, at which moment the angular velocity is high. However, for most of the time, the model predicts nearly symmetric (with respect to the long axis of the bead) distributions of both ActA and actin, and lower angular velocities. We hypothesize that this quantitative discrepancy between the observations and modeling predictions is because we have very simple detachment kinetics of the actin-ActA links in our model. More complex and nonlinear force-dependence of respective detachment rates can, in principle, lead to a much discussed 'stick-slip' properties of the attachments. More specifically, actin-ActA links can detach cooperatively, not one by one, but all at once, so the bead at any given moment is either attached in many places to the actin network, or is almost detached, and there is a rapid back and forth switching between these two states. Indirect data from two studies has pointed to such kinetics [10,11]. If this is indeed the case, a spatial separation during the

fraction of the time the bead is attached would occur and rapid turning would ensue, as described above. This turning would lead to a skewed actin distribution. The resulting positive feedback between actin redistribution, turning and attachment state could lead to the turning state becoming steady and persistent. In our current model this does not happen, but preliminary estimates show that this can happen if the force-dependence of the detachment rate is more nonlinear. We will explore this possibility in the future. Also, it is very likely that if ActA is immobile, any inhomogeneous distribution at the bacterial or bead's surface will cause rapid turns.

References

1. Goldstein H, Poole C, Safko J (2001) Classical mechanics. 3rd ed. Addison-Wesley.
2. Mogilner A, Oster G (2003) Force generation by actin polymerization II: The elastic ratchet and tethered filaments. Biophys J, 84: 1591-1605.
3. Berg HC (1993) Random Walks in Biology. Princeton, New Jersey: Princeton University Press.
4. Lacayo CI, Pincus Z, VanDuijn MM, Wilson CA, Fletcher DA, et al. (2007) Emergence of large-scale cell morphology and movement from local actin filament growth dynamics. PLoS Biol 5: e233.
5. Noireaux V, Golsteyn RM, Friederich E, Prost J, Antony C, et al. (2000) Growing an actin gel on spherical surfaces. Biophys J 78: 1643-1654.
6. Plastino J, Olivier S, Sykes C (2004) Actin filaments align into hollow comets for rapid VASP-mediated propulsion. Curr Biol 14: 1766-1771.
7. Sekimoto K, Prost J, Julicher F, Boukellal H, Bernheim-Grosswasser A (2004) Role of tensile stress in actin gels and a symmetry-breaking instability. Eur Phys J E Soft Matter 13: 247-259.
8. Dickinson RB, Caro L, Purich DL (2004) Force generation by cytoskeletal filament end-tracking proteins. Biophys J 87: 2838-2854.
9. Dayel MJ, Akin O, Landeryou M, Risca V, Mogilner A, Mullins RD (2009). In silico reconstitution of actin-based symmetry breaking and motility. PLoS Biol, 7: e1000201.
10. Soo FS, Theriot JA. (2005) Adhesion controls bacterial actin polymerization-based movement. Proc Natl Acad Sci U S A. 102:16233-16238.
11. Alberts JB, Odell GM. 2004. In silico reconstitution of Listeria propulsion exhibits nano-saltation. PLoS Biol. 2:e412.

Fig. i

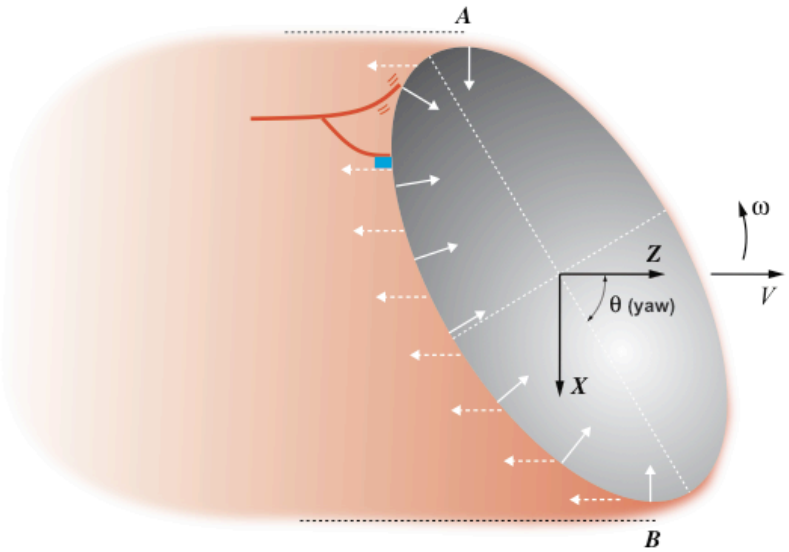

Figure i: Schematic illustration of the model. An ellipsoidal bead is represented by an ellipse with an aspect ratio of 2. Attached filaments apply forces that are on average opposite to the direction of movement and parallel to the comet tail (white dashed arrows). Pushing filaments generate forces directed normal to the surface of the bead (white solid arrows). Bent elongating filaments (top red line) 'drum' on the surface of the bead as a result of Brownian motion and create a pressure directed normal to the surface. Pulling filaments (bottom red line) can transiently attach to molecular complexes (blue rectangle) on the surface creating forces that oppose the forward movement of the bead. Yaw angle=θ, angular velocity=ω, V=speed, A and B are side-to-side comet tail boundaries.

Fig. ii

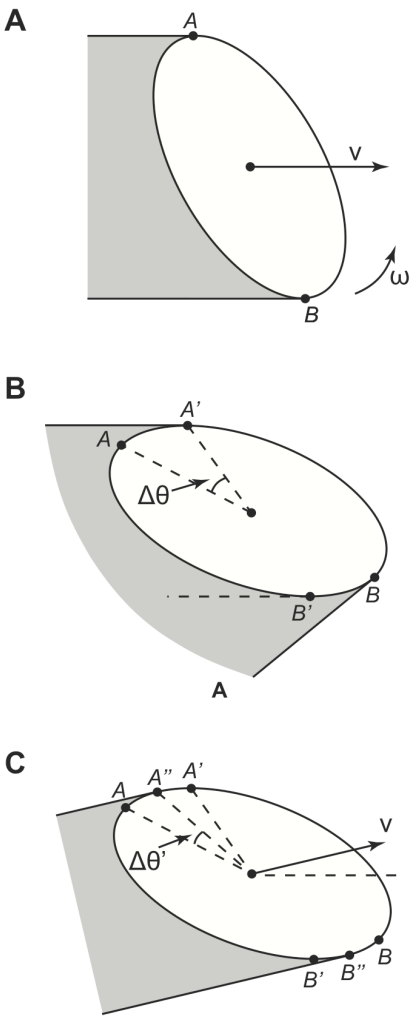

Figure ii: Schematic illustration of the tail's rotation. (A) Before the bead's rotation, points *A* and *B* – edges of the tail – are on opposite sides, on the left and right of the bead. In this schematic the bead is depicted migrating from left to right with a linear speed *V*. Δt represents the time interval. The bead changes direction of movement with the rate ω in the counterclockwise direction. (B) As the bead changes direction, the bead also rotates by the angle $\Delta\theta = \omega\Delta t$ in the counterclockwise direction. In this intermediate stage, point *A* moves to *A′*, while point *B* stays at the same position on the surface of the bead. (C) The tail 'shrinks' so that its new edges, points *A″* and *B″* determining the direction of motion, do not hinder the bead's propulsion.

Fig. iii

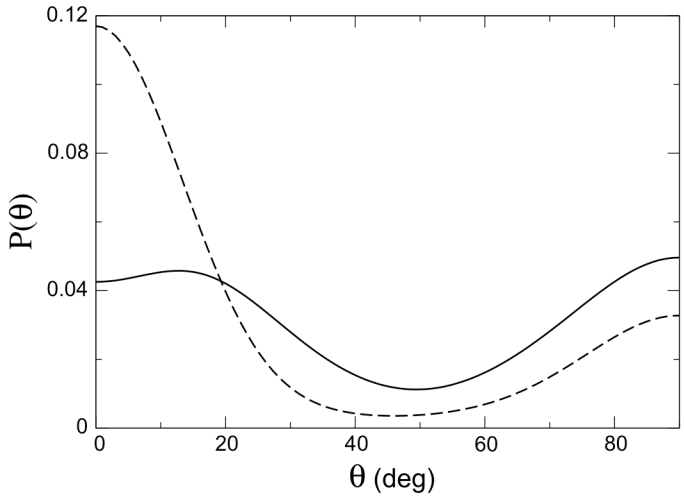

Figure iii: Computed distribution of yaw angles for uncoated (solid line) and lipid-coated beads (dashed line) in the 3D model.

Fig. iv

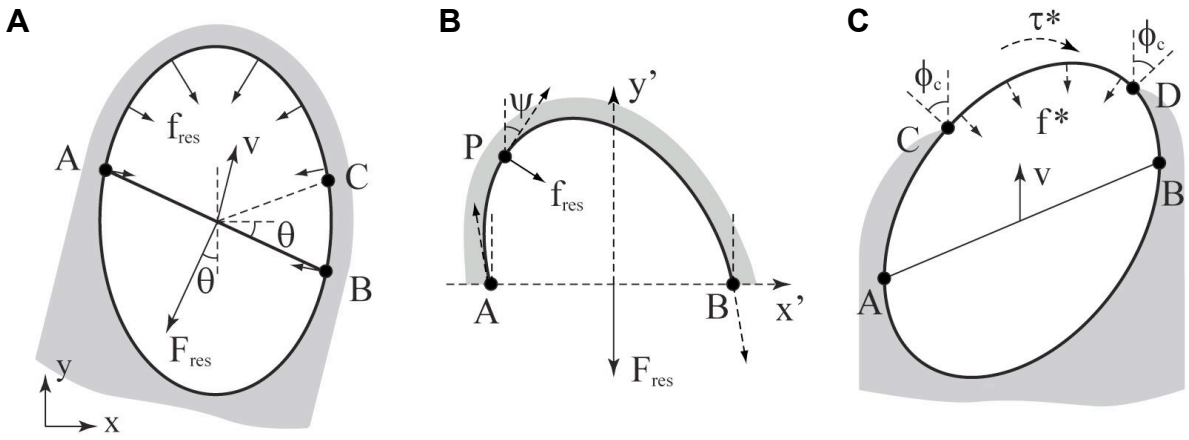

Figure iv: Influence of the actin gel at the front of the bead. (A) Schematic of an ellipsoidal bead surrounded by a uniform gel, including the front of the bead is shown in bead frame-of-reference. A and B are points on the bead where tangents are parallel to v. (B) The front half of the gel in the x'-y' frame-of-reference. (C) Partial actin gel at the front in the tail frame-of-reference. The actin gel exists only if the angle between the surface normal and v is greater than a critical angle ϕ_c (between C and D). The torque from the missing actin gel between C and D is τ*.